

# SCIENTIFIC REPORTS

OPEN

## Computational Prediction of One-Step Synthesis of Seven-membered Fused Rings by (5+2) Cycloaddition Utilising Cycloalkenes

Received: 27 October 2014

Accepted: 23 June 2015

Published: 22 July 2015

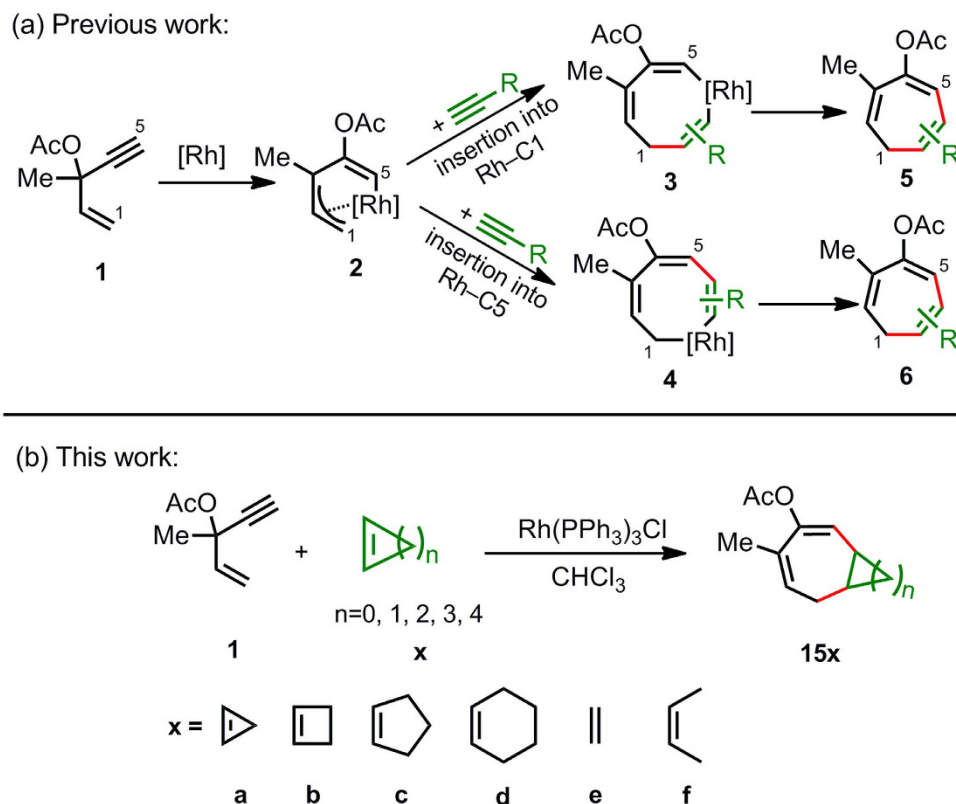
Chen-Chen Zhou, Xiao-Na Ke &amp; Xiu-Fang Xu

The (5+2) cycloaddition reaction utilising cycloalkenes is rare, although it is one of the most efficient methods of constructing seven-membered fused rings because of its high atom- and step-economy. In this study, we used quantum mechanical calculations to predict the plausibility of using the Rh-catalysed intermolecular (5+2) cycloaddition of 3-acyloxy-1,4-enynes and cycloalkenes to produce fused seven-membered carbocycles. The calculation results suggest a convenient, highly efficient and energetically practical approach. Strained cycloalkenes, such as cyclopropene, have been predicted to be active, and the desired bicyclic product should be favoured, accompanied by the formation of byproducts from rearrangement reactions. The energy barriers of the alkene insertion step were analysed by the distortion/interaction model to disclose the origins of the different reactivities of cycloalkenes with different ring sizes.

The construction of seven-membered fused rings has been an important issue in the synthesis of natural products and the development of new medicines<sup>1</sup>. Generally, these bicyclic compounds can be constructed through ring closure of monocyclic compounds<sup>2,3</sup>, rearrangement reactions<sup>4-7</sup>, intramolecular cycloaddition of five-carbon synthons bearing a tethered alkyne<sup>8-12</sup> or modification of previously formed seven-membered rings<sup>13</sup>. However, these methods typically require complicated reactants with subtly positioned functional groups, a substantial amount of organic solvents, and a lengthy course or several synthesis and separation steps. Recently, a number of pericyclic (5+2) cycloadditions have been reported<sup>14</sup>, which provide the possibility of synthesising seven-membered fused ring compounds through the one-step intermolecular (5+2) cycloadditions of a five-carbon synthon and cycloalkenes.

Detailed DFT studies from Houk, Wender and co-workers have revealed that the catalytic cycle of the Rh-catalysed (5+2) reaction of vinylcyclopropane (VCP) with alkynes involves initial cyclopropane ring opening, alkyne insertion and reductive elimination, in which alkyne insertion is found to be not only rate determining but also regioselectivity determining<sup>15-19</sup>. More recently, we have investigated the mechanism of the Rh-catalysed (5+2) reaction of 3-acyloxy-1,4-enynes (ACE) with alkynes (Fig. 1a)<sup>20</sup>, suggesting that this reaction proceeds via three steps, i.e., acyloxy migration, alkyne insertion ( $2\pi$  insertion) and reductive elimination. Therein, the acyloxy migration is rate determining, and the alkyne insertion is regioselectivity determining. Interestingly, alkyne prefers to insert into a rhodium-allyl bond in the VCP-based (5+2) cycloadditions, but prefers to insert into a Rh-C(sp<sup>2</sup>) bond in the ACE-based (5+2) cycloadditions. This difference of mechanism results in not only different regiochemical control but also unique substituent effects on reactivity, when employing ACE instead of VCP as the 5-C

Department of Chemistry, Key Laboratory of Advanced Energy Materials Chemistry (Ministry of Education), Nankai University, Tianjin, 300071, P. R. China. Correspondence and requests for materials should be addressed to X.-F.X. (email: [xxfang@nankai.edu.cn](mailto:xxfang@nankai.edu.cn))

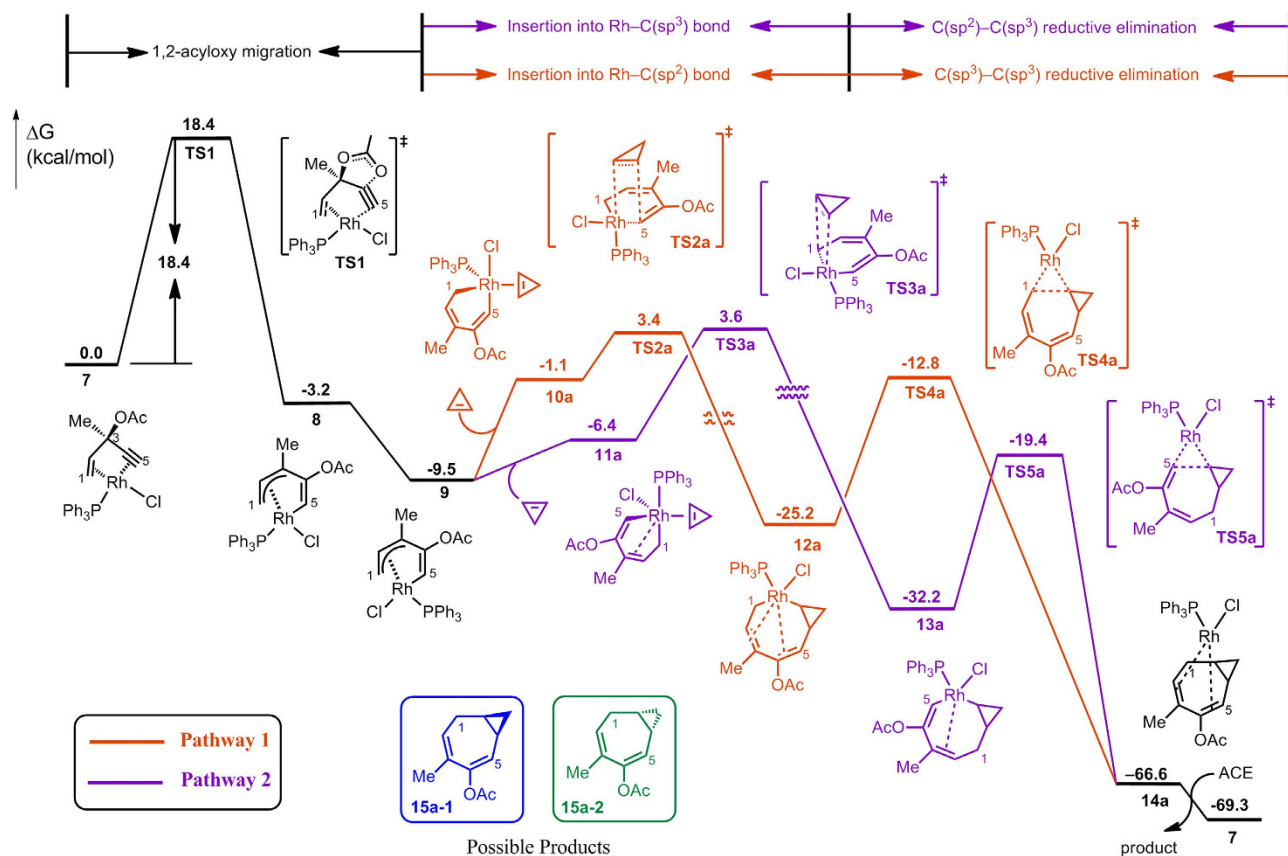


**Figure 1. Proposed mechanisms.** (a) Rh-catalysed (5+2) cycloadditions of 3-acyloxy-1,4-enyne (ACE) and alkynes. (b) Rh-catalysed (5+2) cycloadditions of 3-acyloxy-1,4-enyne (ACE) and alkenes.

synthon. In this study, we attempt to extend the scope of the two-carbon synthon to cycloalkenes, aiming to develop the most atom- and step-economical method to synthesise a fused bicyclic carbon skeleton including a seven-membered ring (Fig. 1b). Significantly, our computational results indicate that the rate-determining step for (5+2) cycloaddition between ACE and cycloalkene varies with the cycloalkene substrate.

ACE is selected as the model five-carbon synthon because its cycloaddition products possess two C=C double bonds that could be selectively functionalised. Density functional theory (DFT) methods are employed to compute this catalytic system because they better balance the computational costs and chemical accuracy<sup>21</sup>. The most efficient catalyst for alkynes, Rh(PPh<sub>3</sub>)<sub>3</sub>Cl, is used as the model catalyst, which releases two phosphine ligands and binds to ACE to initiate the reaction<sup>20</sup>.

The highly strained cyclopropene structure can be used as an excellent three-carbon component to construct six- or five-membered ring skeletons in the Rh(I)-catalyzed [3+2+1] or [3+2] cycloadditions of ene- and yne-cyclopropene systems<sup>22–24</sup>. Wender and coworkers firstly employed vinylcyclopropene as a five-carbon component in the Rh(I)-catalyzed intermolecular [5+2+1] carbocyclization<sup>25</sup>. Small cycloalkenes, namely cyclopropene<sup>26,27</sup>, cyclobutene and their derivatives<sup>28</sup>, have been reported to show a high reactivity in Diels-Alder reactions. Recent studies from the Houk group<sup>28,29</sup> have accounted for this unusual high reactivity of strained cycloalkenes by a distortion/interaction model<sup>30</sup>. Because of the strain, the cycloalkene is pre-distorted to reduce the distortion energy, therefore lowering the overall activation energy. Both experimental<sup>10,11,31</sup> and theoretical<sup>20</sup> studies have suggested that Rh-catalysed (5+2) reaction of ACEs with alkynes proceeds via sequential steps of acyloxy migration, alkyne insertion (2 $\pi$  insertion) and reductive elimination. Because the 2 $\pi$  insertion step in the (5+2) cycloadditions is a bimolecular pericyclic process, similar to the Diels-Alder reaction, we expect that the cycloalkenes will also act as potential two-carbon synthons for Rh-catalysed (5+2) cycloaddition with ACE. Therefore, we envisioned that the designed (5+2) cycloadditions of ACE and cycloalkenes might take place via the same three steps, as the (5+2) cycloadditions of ACE and alkynes do. It is noteworthy that the two-carbon synthon is not involved in the initial acyloxy migration but in the following 2 $\pi$  insertion and reductive elimination two steps (Fig. 1a). As a result, if the cycloalkene substrates have similar reactivities to the alkynes in the latter two steps, the reaction should be plausible, at least theoretically. Cycloalkenes with different ring sizes are employed in the calculations as well as open-chain alkenes for comparison (Fig. 1b).



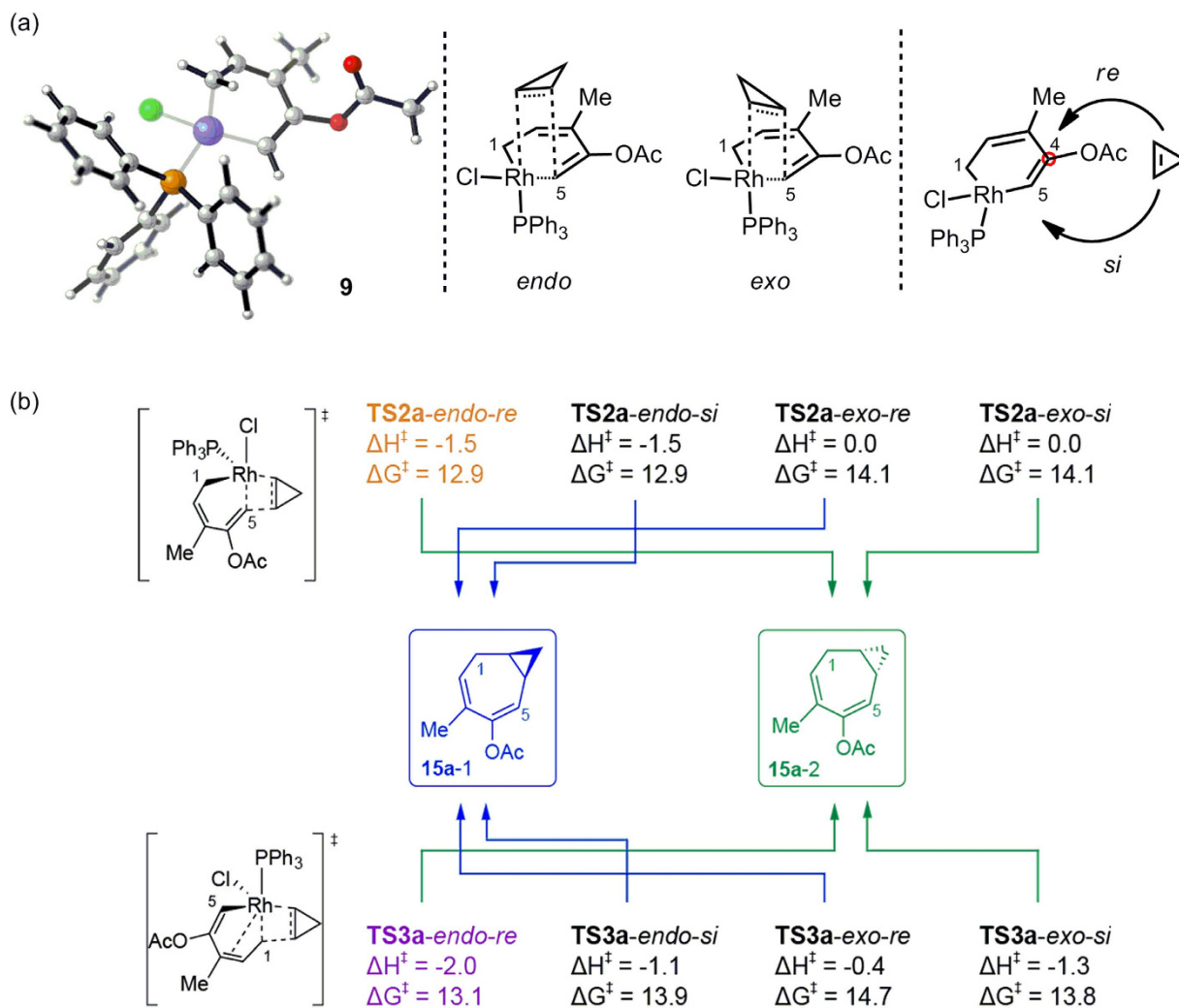
**Figure 2.** Two of the representative pathways of Rh-catalysed (5+2) cycloadditions of ACE and cyclopropene.

## Results and Discussion

Two of the typical pathways of cycloaddition with cyclopropene are computed and presented in Fig. 2. The reaction is initiated at the ACE-Rh(PPh<sub>3</sub>)Cl  $\pi$  complex **7**<sup>20</sup>. The acyloxy group migrates from C3 to C4 through a five-membered ring transition state (TS1) with a barrier of 18.4 kcal/mol. The resulting complex **8** can convert into a more stable isomer **9** by exchanging the two ligands Cl and PPh<sub>3</sub>. The cycloalkene substrate could then be inserted into the metallacycle from either the Rh-C5(sp<sup>2</sup>) bond (pathway 1) or the Rh-C1(sp<sup>3</sup>) bond (pathway 2). The intermediates **12a** and **13a** from either of the 2 $\pi$  insertion pathways will undergo reductive elimination to generate the product complex **14a**, which then releases the product while rebinding to ACE, thus completing a catalytic cycle.

The conformation of the alkene insertion (2 $\pi$  insertion) step determines the chirality of the products. Intermediate **9** is a slightly twisted metallacycle. The cycloalkene could approach metal complex **9** in an *endo* or *exo* orientation to the metallacycle ring (Fig. 3a). The cycloalkene could also bind to the rhodium centre from both sides of the ring plane. To distinguish the two sides of the metallacycle, the conventional nomenclature of the pro-chirality of sp<sup>2</sup> carbons is applied to this system, and the two different orientations are named *re* and *si* according to the pro-chirality of C4 of ACE (Fig. 3a). All of the orientations of the cyclopropene insertion were considered. The corresponding energy barriers are listed in Fig. 3b, and the transition states for the *re* insertion patterns are shown in Fig. 4a. Noticeably, these approaches with different orientations will lead to fused ring products with different chirality (**15a-1** and **15a-2** in Fig. 3b).

It was found that when cyclopropene inserts into the Rh-C5(sp<sup>2</sup>) bond (TS2a), the rhodium metallacycle in TS2a is generally planar, causing the *re* and *si* orientations to be more chemically and energetically similar, while the *endo* and *exo* orientations show a larger difference in energy. Generally, the *endo* transition states are lower in energy than the *exo* transition states, which is consistent with the previously reported results<sup>32,33</sup>. The energy difference between the *endo*- and *exo*-TSs is mainly caused by two factors. An examination on the geometries of the *endo* and *exo* transition states of the cyclopropene insertion reveals that, in the transition state TS2a-*endo-re*, the methylene hydrogen of cyclopropene is positioned toward the C2=C3 double bond (Fig. 4a), which will result in the CH- $\pi$  interaction between the methylene hydrogen of cyclopropene and the C2=C3 double bond. However, in the transition state TS2a-*exo-re*, the methylene hydrogen of cyclopropene is positioned backward the five-carbon skeleton

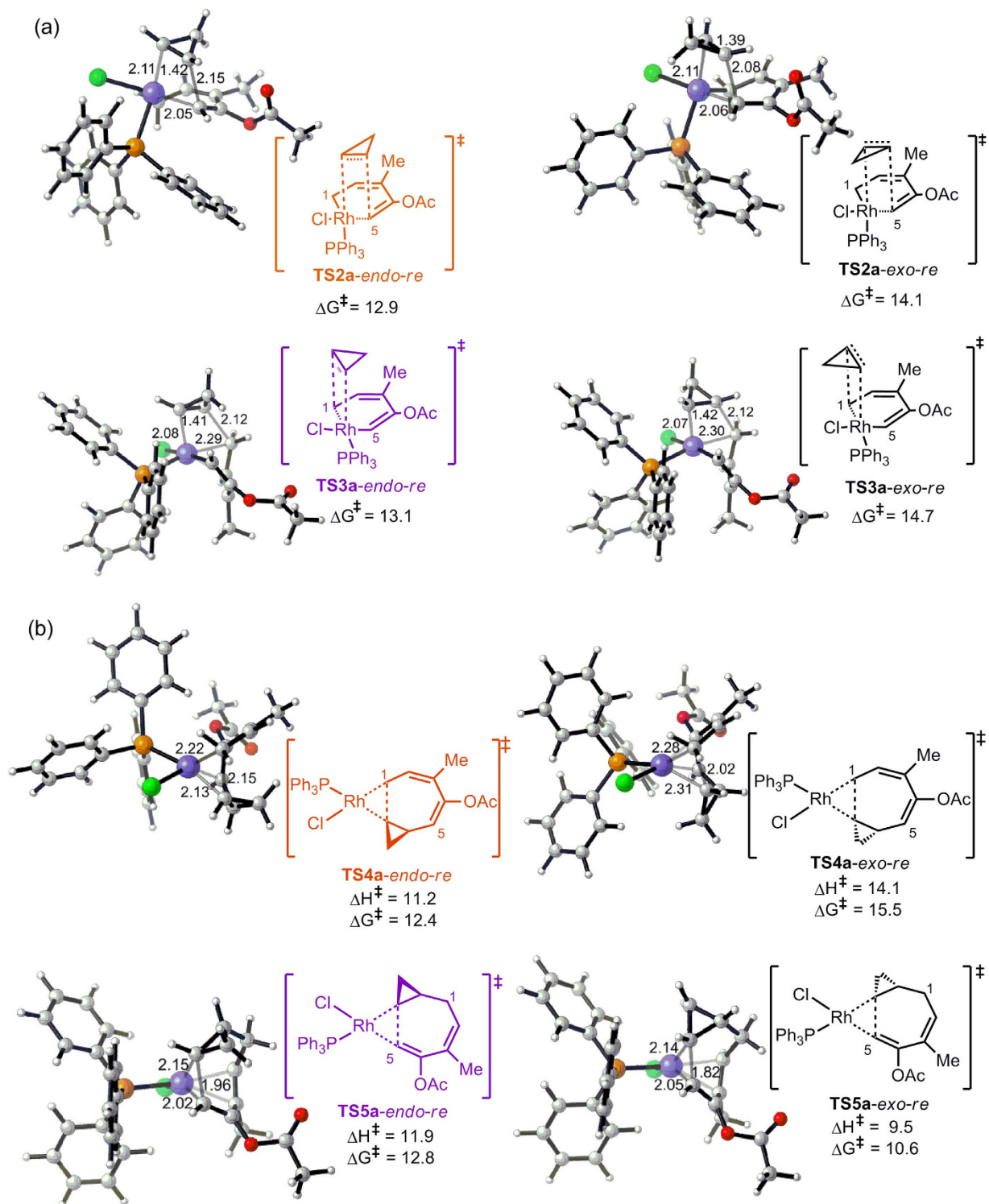


**Figure 3.** (a) The 3D model of intermediate 9 and the possible patterns for cyclopropene insertion. (b) Energy barriers for the various cyclopropene insertion transition states. Energy barriers are calculated relative to intermediate 9 in kcal/mol. The transition states TS2a and TS3a presented in Fig. 1 are highlighted accordingly (in orange and in purple). Blue and Green arrows indicate to which enantiomer the transition state will lead.

of ACE moiety (Fig. 4a). As a result, no CH- $\pi$  interaction could be observed in **TS2a-exo-re**. Therefore, the CH- $\pi$  interaction between the methylene hydrogen of cyclopropene and the C2=C3 double bond may be one of the main factors contributing to the lower energy of the *endo* transition state of the cyclopropene insertion relative to that of the *exo* transition state. Moreover, the consistent results obtained by the M06 and ONIOM methods<sup>34–37</sup> confirmed that the stronger steric repulsion between the bulky PPh<sub>3</sub> ligand and the cyclopropene in *exo*-TSs than in *endo*-TSs is the other factor contributing to the energy difference between *endo*- and *exo*-TSs (for details, see Table S1 in the Supporting Information). For the insertion of cyclopropene into the Rh-Cl(sp<sup>3</sup>) bond (**TS3a**), the rhodium metallacycle is relatively more twisted because C1 must be sp<sup>3</sup> hybridised to bind with the cyclopropene substrate. In that case, the two faces of the metallacycle are more chemically different and possess less orbital overlap with the cyclopropene substrate. This trend is clearly observed in the calculated energy barriers, as shown in Fig. 3b in which in **TS2a**, the *re/si* insertion barriers are identical, while in **TS3a**, the *re/si* insertion barriers are different.

All of the calculated cyclopropene insertion barriers (12.9–14.7 kcal/mol, Fig. 3b) are lower than that of the 1,2-acyloxy migration, regardless of the approach of cyclopropene to the rhodium complex. This result indicates that the cyclopropene insertion step should not be rate determining. However, the differences between the barriers of the favoured 2 $\pi$  insertion patterns (for example, **TS2a-endo-re** and **TS2a-endo-si**) are small because the *re* and *si* orientations are nearly mirror images. Thus, the reaction is not likely to be stereo-selective. However, it is expected that the introduction of chiral factors,





**Figure 4. Geometries of the transition states for the cyclopropene insertion and reductive elimination steps.** (a) Geometries of four possible transition states for the *re* cyclopropene insertion. **TS2a-endo-re** and **TS3a-endo-re** are the two transition states **TS2a** and **TS3a** shown in Fig. 1. Energy barriers are in kcal/mol and calculated relative to intermediate **9**. The four possible transition states for the *si* cyclopropene insertion are given in Figure S1 of the Supplementary Information. (b) Geometries of four reductive elimination transition states. **TS4a-endo-re** and **TS5a-endo-re** are the two transition states **TS4a** and **TS5a** shown in Fig. 1. Activation enthalpies and Gibbs free energies are in kcal/mol and calculated relative to the corresponding metallacycle intermediate **12a** and **13a**, respectively.

such as chiral ligands or asymmetrically substituted cycloalkenes, to the reaction system will lead to stereo-selectivity.

For clarity, the following discussions will only consider pathways involved with the *re* patterns of the  $2\pi$  insertion. The expanded eight-membered metallacycle intermediates **12a** and **13a** then undergo reductive elimination to generate the product complex **14a**. As shown in Fig. 2, **TS4a** and **TS5a** are the two reductive elimination transition states in the two different pathways. Generally, **TS4a** is higher in energy than **TS5a** because in **TS4a**, a C(sp<sup>3</sup>)-C(sp<sup>3</sup>) bond is formed, while in **TS5a**, a C(sp<sup>2</sup>)-C(sp<sup>3</sup>) bond is formed. The reductive elimination energy barriers are also generally low (10.6–15.5 kcal/mol, Fig. 4b); therefore, the rate-determining step is acyloxy migration for the (5+2) reaction with cyclopropene.

For the product complex **14a**, ACE binds with rhodium, releasing the product, thus, completing a catalytic cycle. The exchange energy of ACE and of the product is negative (−2.7 kcal/mol), which suggests that the regeneration of Rh-ACE complex **7** is favoured. The exchange energy is noteworthy because if the product complex is more stable while the first step is rate determining, then the overall activation barrier will be elevated according to the energy span model<sup>38</sup>. Negative exchange energy ensures that the catalytic cycle would proceed easily.

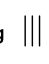



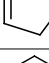
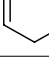
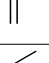
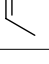
Due to the extreme strain of the cyclopropene ring, the C-C bond of the three-membered ring is less stable than open-chain alkenes, and the induction of possible rearrangement reactions is discussed in the supplementary information (Figures S2 and S3). The overall energy profile shows that these rearrangements are less favoured and should not affect the generation of the seven-membered fused ring product.

Typically, synthesized cyclopropenes have at least two substituents<sup>27,39,40</sup>. The presence of these substituents facilitates the use of these cycles and the synthesis. In this study, we computed the activation barrier of the cyclopropene insertion step for a substituted cyclopropene **a'**. The results are listed in entry **a'** of Table 1. As expected, the activation barrier for cyclopropene insertion of the substituted cyclopropene **a'** increased to 21.0 kcal/mol (the  $2\pi$  insertion step). This result should be primarily attributed to steric repulsion between substituents on cyclopropene and the bulky PPh<sub>3</sub> ligand (see Figure S4 in the Supporting Information). Because an activation barrier of 21.0 kcal/mol is not high, the reaction with the substituted cyclopropene is predicted to occur using a higher temperature.

Energy profiles of the reactions with cycloalkenes of different sizes were calculated, and the most favoured pathways are listed in Table 1. From the calculated energies (Table 1), it can be observed that in most cases, pathway 1 is more favoured in the  $2\pi$  insertion step, while pathway 2 is more favoured in reductive elimination. As the size of the cycloalkene ring increases, the energy barrier of the  $2\pi$  insertion step also increases. The  $2\pi$  insertion step is obviously influenced by the ring size of the cycloalkenes, while this trend is not observed for reductive elimination.

As the substrate changes, the rate-determining step also varies. Table 1 indicates that the rate-determining step is sensitive to the 2-carbon synthon. This result is primarily attributed to a combination of three factors: the steric repulsion between two substrates as well as that between substrates and the bulky PPh<sub>3</sub> ligand, the distortion energy for the 2-carbon synthon to achieve the transition-state geometry, and the electronic effect of the 2-carbon synthon. Steric repulsion becomes stronger as the size of the 2-carbon synthon increases, thus leading to higher energy barriers of the  $2\pi$  insertion and the reductive elimination steps. Therefore, the transition states of the  $2\pi$  insertion or reductive elimination reach the highest point of the energy profile and become the rate-determining step. For example, the rate-determining step for the reaction with cyclobutene is the  $2\pi$  insertion and that for cyclopentene is reductive elimination, while that for cyclopropene is acyloxy migration (entries a, b and c). Similarly, introduction of substituents to the 2-carbon synthon will also increase the activation barrier of the  $2\pi$  insertion step due to increased steric repulsion. For example, the activation barrier of the  $2\pi$  insertion for substituted cyclopropene **a'** is 21.0 kcal/mol (entry **a'**), which is 2.6 kcal/mol higher than that of the 1,2-acyloxy migration; therefore, the  $2\pi$  insertion is the rate-determining step for this substituted cyclopropene. As illustrated in Fig. 5, the distortion energies required for cycloalkenes to achieve the transition-state geometries of the  $2\pi$  insertion increase as the size of the cycloalkenes increases, leading to an increase of the activation barriers of the  $2\pi$  insertion step. For example, the transition state of the  $2\pi$  insertion for cyclohexene has the highest free energy; therefore, it is the rate-determining step. Generally, because alkene substrates are less electron-rich than alkyne substrates, the  $2\pi$  insertion of an alkene requires a higher activation energy than that required for an alkyne. For example, the rate-determining step is the  $2\pi$  insertion with an activation barrier of 20.5 kcal/mol for ethylene, (entry e). The activation barrier of the  $2\pi$  insertion for acetylene is 14.2 kcal/mol, which is 4.2 kcal/mol lower than that of the 1,2-acyloxy migration (entry g). Therefore, the 1,2-acyloxy migration is the rate-determining step for acetylene.

The overall activation energy increases with the size of the cycloalkene ring. According to the overall activation free energies (the highlighted  $\Delta G^\ddagger$ ) listed in Table 1, cyclopropene should be as reactive as acetylene in this reaction, while cyclobutene may be as reactive as ethylene. Cyclopentene and cyclohexene are less reactive because of their larger ring size, similar to the open chain *cis*-2-butene. Therefore, our calculation results suggest that intermolecular (5+2) cycloaddition of ACE with cyclopropene should be plausible because acetylene and substituted acetylenes are good reactants for this type of reaction<sup>10</sup>. Reactions with cyclobutene might proceed by heating the reaction system to a higher temperature, while it will be more difficult for reactions with cyclopentene or cyclohexene to proceed under moderate conditions.

2 $\pi$ substrate <b>x</b>	Acyloxy Migration <sup>c</sup>		Pathway <sup>b</sup>	2 $\pi$ Insertion <sup>d</sup>		Reductive Elimination <sup>e</sup>		Exchange Energy <sup>f</sup>	
	$\Delta H^\ddagger$	$\Delta G^\ddagger$		$\Delta H^\ddagger$	$\Delta G^\ddagger$	$\Delta H^\ddagger$	$\Delta G^\ddagger$	$\Delta H$	$\Delta G$
<b>g</b> 	16.8	18.4	1(favoured)	2.3	14.2	13.4	14.4	-3.2	-2.8
			2	8.9	21.2	1.9	3.1		
<b>a</b> 	16.8	18.4	1(favoured)	-1.5	12.9	11.2	12.4	-3.1	-2.7
			2	-2.0	13.1	11.9	12.8		
<b>a'</b> 	16.8	18.4	1(favoured)	8.5	21.0	12.8	14.2	-4.7	-5.0
<b>b</b> 	16.8	18.4	1	5.7	20.6	16.8	18.1	-1.9	-1.8
			2(favoured)	5.1	20.4	14.6	15.5		
<b>c</b> 	16.8	18.4	1(favoured)	5.1	20.9	21.5	22.1	-9.6	-9.2
			2	7.4	23.4	14.9	16.0		
<b>d</b> 	16.8	18.4	1(favoured)	10.4	25.4	16.2	17.6	-1.2	-1.3
			2	12.5	28.1	20.0	20.9		
<b>e</b> 	16.8	18.4	1(favoured)	7.1	20.5	14.0	15.1	1.7	2.2
			2	6.8	21.2	15.9	16.6		
<b>f</b> 	16.8	18.4	1	9.8	24.8	17.3	18.7	-1.7	-1.5
			2(favoured)	8.4	24.4	13.7	14.5		

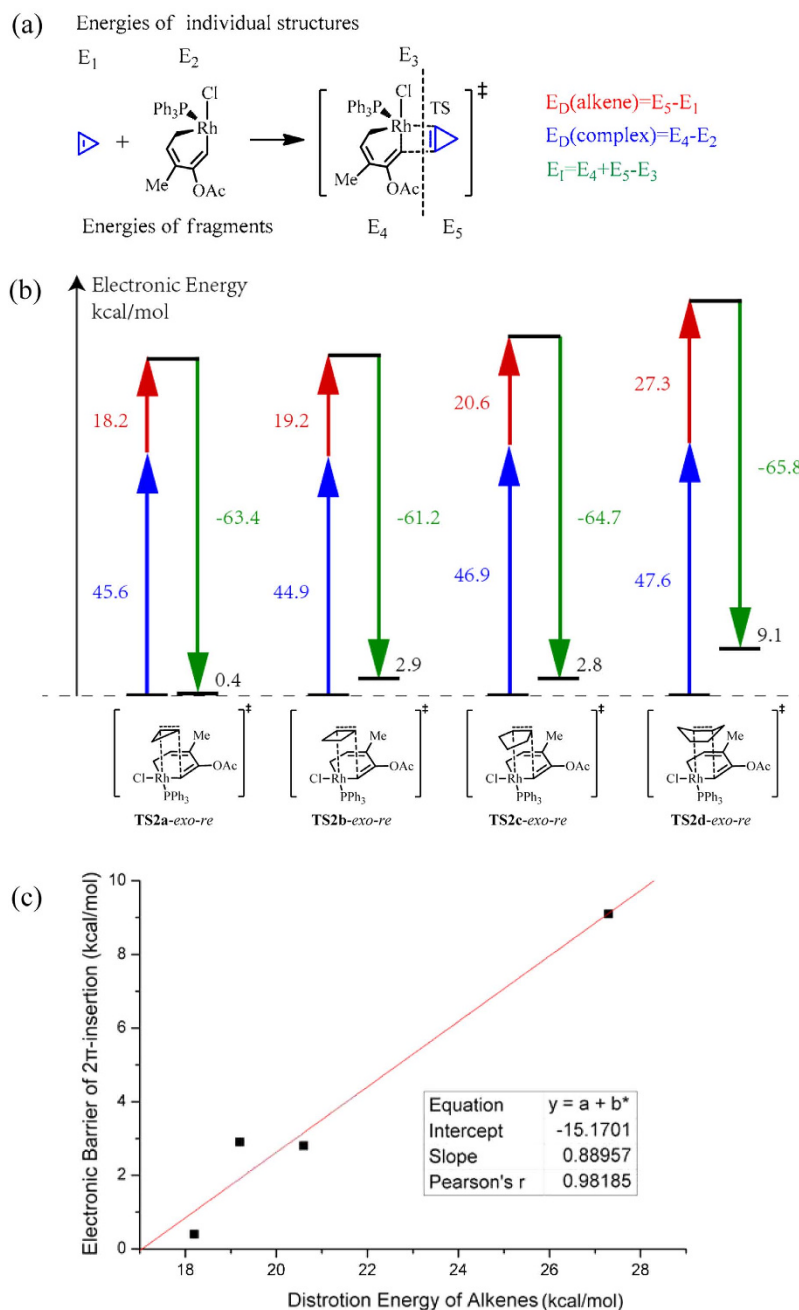
**Table 1.** Calculated activation enthalpies ( $\Delta H^\ddagger$ ) and activation free energies ( $\Delta G^\ddagger$ ) of the most favoured pathways for the (5+2) cycloadditions of ACE 1 with a series of 2 $\pi$  substrates (acetylene, cycloalkenes, ethylene, *cis*-2-butene)<sup>a</sup>. <sup>a</sup>All energies are in kcal/mol. <sup>b</sup>Pathway 1 is the 2 $\pi$  insertion into Rh-C5(sp<sup>2</sup>) and Pathway 2 is the 2 $\pi$  insertion into Rh-C1(sp<sup>3</sup>) bond. <sup>c</sup>Activation energy of acyloxy migration, same for all of the 2 $\pi$  substrates, is calculated relative to **7**. <sup>d</sup>Activation energy of the 2 $\pi$  insertion step is calculated relative to the acyloxy migration product **9**, and <sup>e</sup>reductive elimination relative to the corresponding insertion product **12x** or **13x** (**x** = **a**, **b**, **c**, **d**, **e**, **f**, **g**). <sup>f</sup>Exchange energy is the energy difference of Rh-ACE complex plus the product and Rh-product complex plus ACE. The activation free energies of the rate-determining step are highlighted.

As discussed above, the 2 $\pi$  insertion step is obviously influenced by the ring size of the cycloalkenes. In this study, the distortion/interaction (D/I) model<sup>30</sup> is applied to the 2 $\pi$  insertion step according to the following partitioning scheme (Fig. 5a) to investigate the origins of the different reactivities displayed by the substrates. To compare the distortion energies of the rhodium complex fragments ( $E_D(\text{complex})$ ), the same geometry (**TS2x-*exo-re***, **x** = **a**, **b**, **c** and **d**) of the transition states for the 2 $\pi$  insertion are adopted for different substrates in the analysis.

From the D/I analysis (Fig. 5b), we can observe that the activation barrier is significantly related to the distortion energy of the cycloalkene substrate ( $E_D(\text{alkene})$ ). The variations in distortion energy of the metallacycle ( $E_D(\text{complex})$ ) and the interaction energy ( $E_I$ ) are relatively small for different substrates. The linear fitting (Fig. 5c) of the electronic energies of activation and the distortion energies of the alkenes has a correlation coefficient of 0.98, also proving that the two quantities are related. The energies required for cycloalkenes to be distorted into the 2 $\pi$  insertion transition states increase as the ring size of the cycloalkenes increases from cyclopropene to cyclohexene, resulting in an increase in the activation barriers. This correlation is the same as that observed in the Diels-Alder cycloaddition<sup>29</sup>, and we suppose it may also occur in other pericyclic reactions.

## Conclusion

In this study, we explored the plausibility of the Rh-catalysed (5+2) cycloaddition reaction between ACE and cycloalkenes. The more strained cycloalkenes are predicted to be more reactive in this reaction, while those with a larger ring are less reactive. Cyclopropene is suggested to be as reactive as acetylene and is a potential reagent; cyclobutene is less reactive, but the reaction may be practical at a higher temperature. The rate-determining step varies with different cycloalkenes primarily because of the change of the energy barrier of the 2 $\pi$  insertion step. The distortion/interaction model was introduced to disclose the origins of the different reactivities of various cycloalkenes. The distortion of the alkene was found to be the primary factor influencing the reactivity. The reaction follows the mechanism of the (5+2) cycloaddition between ACE and alkynes and is stereochemically complicated in the cycloalkene insertion step. It is expected that stereo-selectivities might be realised by introducing chiral factors to the reaction systems.



**Figure 5. Distortion/Interaction (D/I) analysis of the 2 $\pi$  insertion step for different substrates.** (a) The energy partitioning scheme for the D/I analysis. (b) The distortion energies and interaction energies. Red arrows indicate the distortion energies of alkenes, blue arrows indicate the distortion energies of the metallacycle fragments, and green arrows indicate the interaction energies. The overall electronic energies of activation are shown in black. Energy values are given in kcal/mol. (c) Linear fitting between electronic energies of activation and the corresponding distortion energies of the cycloalkenes for the 2 $\pi$  insertion step.

## Methods

All of the calculations were performed using the Gaussian 09 software package. Geometry optimisations were performed with the B3LYP<sup>41–43</sup> functional. The Stuttgart/Dresden effective core potential<sup>44</sup> was used on rhodium, and the 6–31G(d) basis set was employed for other atoms. We considered all of the possible isomers by rotating the bulky PPh<sub>3</sub> group around the Rh–P bond and rotating the acyloxy group around the C3–O bond for the conformation search and, finally, screening out the most stable isomer for each species. The isomers with the lowest energy are presented. Frequency calculations were performed at 298.15 K to verify that the stationary points were the local minima or first-order saddle points, i.e., transition states, and to obtain thermal corrections. The harmonic oscillator approximation engaged in



vibrational frequency calculations were replaced by Truhlar's quasi-harmonic approximation<sup>45</sup>. Intrinsic Reaction Coordinate (IRC) calculations were performed to determine the connectivity of the minima and transition states. Single point energy calculations were performed with the M06 functional<sup>46</sup>, a mixed basis set of SDD for rhodium and 6-311+G(d, p) for other atoms, and the SMD<sup>47</sup> solvation model with chloroform as the solvent ( $\epsilon = 4.7113$ ). Enthalpy and Gibbs free energy values are the sum of the electronic energy from the single point calculations and the thermal corrections obtained by the frequency calculations.

Because the molecular systems in this study are relatively large, dispersion effects may be important. To address this issue, we selected entry d as the test case and performed the DFT-D3 correction<sup>48,49</sup> with M062X functional<sup>50</sup>. The results are listed in Table S4 of the Supporting Information. The results confirm that our conclusions are reliable based on the M06/SDD-6-311+G(d, p)/SMD(CHCl<sub>3</sub>)/B3LYP/SDD-6-31 G(d) computed energies. Thus, we did not apply the DFT-D3 correction for the remaining entries.

## References

- Butenschön, H. Seven-membered rings by cyclization at transition metals: [4+3], [3+2+2], [5+2]. *Angew. Chem. Int. Ed.* **47**, 5287–5290 (2008).
- Li, W., Yuan, W., Shi, M., Hernandez, E. & Li, G. Rhodium(I)-catalyzed intramolecular ene reaction of vinylidenecyclopropanes and alkenes for the formation of bicyclo[5.1.0] octylenes. *Org. Lett.* **12**, 64–67 (2010).
- Ovaska, T. V., Sullivan, J. A., Ovaska, S. I., Winegrad, J. B. & Fair, J. D. Asymmetric synthesis of seven-membered carbocyclic rings via a sequential oxyanionic 5-exo-dig cyclization/claisen rearrangement process. total synthesis of (–)-frondosin B. *Org. Lett.* **11**, 2715–2718 (2009).
- Sarpong, R., Su, J. T. & Stoltz, B. M. The development of a facile tandem Wolff/Cope rearrangement for the synthesis of fused carbocyclic skeletons. *J. Am. Chem. Soc.* **125**, 13624–13625 (2003).
- Brookhart, M., Davis, E. R. & Harris, D. L. Low-temperature protonation of cyclooctatetraeneiron tricarbonyl and methylcyclooctatetraeneiron tricarbonyl. Generation and observation of cyclooctatrienyliron tricarbonyl cations. *J. Am. Chem. Soc.* **94**, 7853–7858 (1972).
- Bourguet, E. *et al.* Photochemical rearrangement of oxaziridines and nitrones in the hexahydroindole series: A convenient synthetic route to 1-azabicyclo[5.2.0]nonan-2-ones as novel RGD mimetics. *Org. Lett.* **3**, 3067–3070 (2001).
- Radlick, P., Fenical, W. & Alford, G. The synthesis and thermal rearrangement of cis-9-methylenebicyclo [6-1-0]nonene derivatives. *Tetrahedron Lett.* **11**, 2707–2710 (1970).
- Pellissier, H. Recent developments in the [5+2] cycloaddition. *Adv. Synth. Catal.* **353**, 189–218 (2011).
- Wender, P. A., Takahashi, H. & Witulski, B. Transition metal catalyzed [5+2] cycloadditions of vinylcyclopropanes and alkynes: A homolog of the Diels-Alder reaction for the synthesis of seven-membered rings. *J. Am. Chem. Soc.* **117**, 4720–4721 (1995).
- Shu, X.-Z., Huang, S.-Y., Shu, D.-X., Guzei, I. A. & Tang, W.-P. Interception of a rautenstrauch intermediate by alkynes for [5+2] cycloaddition: Rhodium-catalyzed cycloisomerization of 3-acyloxy-4-ene-1,9-diyne to bicyclo[5.3.0]decatrienes. *Angew. Chem. Int. Ed.* **50**, 8153–8156 (2011).
- Shu, X.-Z. *et al.* Rhodium-catalyzed intra- and intermolecular [5+2] cycloaddition of 3-acyloxy-1,4-enyne and alkyne with concomitant 1,2-acyloxy migration. *J. Am. Chem. Soc.* **134**, 5211–5221 (2012).
- Mukai, C., Hara, Y., Miyashita, Y. & Inagaki, F. Thermal [2+2] cycloaddition of allenynes: easy construction of bicyclo[6.2.0] deca-1,8-dienes, bicyclo[5.2.0]nona-1,7-dienes, and bicyclo[4.2.0]octa-1,6-dienes. *J. Org. Chem.* **72**, 4454–4461 (2007).
- Taylor, M. D., Minaskanian, G., Winzenberg, K. N., Santone, P. & Smith, A. B. Preparation, stereochemistry, and nuclear magnetic resonance spectroscopy of 4-hydroxy(acetoxy)bicyclo[5.1.0]octanes. Synthesis of (–)- and (+)-8,8-dimethylbicyclo[5.1.0]oct-2-en-4-one. *J. Org. Chem.* **47**, 3960–3964 (1982).
- Ylijoki, K. E. O. & Stryker, J. M. [5+2] cycloaddition reactions in organic and natural product synthesis. *Chem. Rev.* **113**, 2244–2266 (2012).
- Yu, Z.-X., Wender, P. A. & Houk, K. N. On the mechanism of [Rh(CO)<sub>2</sub>Cl]<sub>2</sub>-catalyzed intermolecular (5+2) reactions between vinylcyclopropanes and alkynes. *J. Am. Chem. Soc.* **126**, 9154–9155 (2004).
- Yu, Z.-X. *et al.* Origins of differences in reactivities of alkenes, alkynes, and allenes in [Rh(CO)<sub>2</sub>Cl]<sub>2</sub>-catalyzed (5+2) cycloaddition reactions with vinylcyclopropanes. *J. Am. Chem. Soc.* **130**, 2378–2379 (2008).
- Liu, P., Cheong, P. H. Y., Yu, Z.-X., Wender, P. A. & Houk, K. N. Substituent effects, reactant preorganization, and ligand exchange control the reactivity in Rh<sup>I</sup>-catalyzed (5+2) cycloadditions between vinylcyclopropanes and alkynes. *Angew. Chem. Int. Ed.* **47**, 3939–3941 (2008).
- Liu, P. *et al.* Electronic and steric control of regioselectivities in Rh(I)-catalyzed (5+2) cycloadditions: Experiment and theory. *J. Am. Chem. Soc.* **132**, 10127–10135 (2010).
- Xu, X.-F. *et al.* Ligand effects on rates and regioselectivities of Rh(I)-catalyzed (5+2) cycloadditions: A computational study of cyclooctadiene and dinaphthocyclooctatetraene as ligands. *J. Am. Chem. Soc.* **134**, 11012–11025 (2012).
- Xu, X.-F., Liu, P., Shu, X.-Z., Tang, W.-P. & Houk, K. N. Rh-catalyzed (5+2) cycloadditions of 3-acyloxy-1,4-enynes and alkynes: Computational study of mechanism, reactivity, and regioselectivity. *J. Am. Chem. Soc.* **135**, 9271–9274 (2013).
- Zhao, Y. & Truhlar, D. G. Density functionals with broad applicability in chemistry. *Acc. Chem. Res.* **41**, 157–167 (2008).
- Li, C. K., Zhang, H., Feng, J. J., Zhang, Y. & Wang, J. B. Rh(I)-catalyzed carbonylative carbocyclization of tethered ene- and yne-cyclopropenes. *Org. Lett.* **12**, 3082–3085 (2010).
- Shibata, T., Maekawa, S. & Tamura, K. Rhodium-catalyzed intramolecular cycloaddition of cyclopropene-ynes triggered by carbon-carbon bond cleavage. *Heterocycles*, **76**, 1261–1270 (2008).
- Zhu, Z.-B., Wei, Y. & Shi, M. Recent developments of cyclopropene chemistry. *Chem. Soc. Rev.* **40**, 5534–5563 (2011).
- Wender, P. A., Gamber, G. G., Hubbard, R. D. & Zhang, L. Three-component cycloadditions: the first transition metal-catalyzed [5+2+1] cycloaddition reactions. *J. Am. Chem. Soc.* **124**, 2876–2877 (2002).
- Wiberg, K. B. & Bartley, W. J. Cyclopropene. V. Some reactions of cyclopropene<sup>1</sup>. *J. Am. Chem. Soc.* **82**, 6375–6380 (1960).
- Lou, Y., Horikawa, M., Kloster, R. A., Hawryluk, N. A. & Corey, E. J. A new chiral Rh(II) catalyst for enantioselective [2+1]-cycloaddition. Mechanistic implications and applications. *J. Am. Chem. Soc.* **126**, 8916–8918 (2004).
- Paton, R. S., Kim, S., Ross, A. G., Danishefsky, S. J. & Houk, K. N. Experimental Diels-Alder reactivities of cycloalkenes and cyclic dienes explained through transition-state distortion energies. *Angew. Chem. Int. Ed.* **50**, 10366–10368 (2011).
- Liu, F., Paton, R. S., Kim, S., Liang, Y. & Houk, K. N. Diels-Alder reactivities of strained and unstrained cycloalkenes with normal and inverse-electron-demand dienes: Activation barriers and distortion/interaction analysis. *J. Am. Chem. Soc.* **135**, 15642–15649 (2013).

30. Ess, D. H. & Houk, K. N. Distortion/interaction energy control of 1,3-dipolar cycloaddition reactivity. *J. Am. Chem. Soc.* **129**, 10646–10647 (2007).
31. Schienebeck, C. M., Robichaux, P. J., Li, X.-X., Chen, L.-Q. & Tang, W.-P. Effect of ester on rhodium-catalyzed intermolecular [5+2] cycloaddition of 3-acyloxy-1,4-enynes and alkynes. *Chem. Commun.* **49**, 2616–2618 (2013).
32. Deng, Q. L., Thomas IV, B. E., Houk, K. N. & Dowd, P. Transition structures of the ene reactions of cyclopropene. *J. Am. Chem. Soc.* **119**, 6902–6908 (1997).
33. Jursic, B. S. A density functional theory study of secondary orbital overlap in endo cycloaddition reactions. An example of a Diels-Alder reaction between butadiene and cyclopropene. *J. Org. Chem.* **62**, 3046–3048 (1997).
34. Dapprich, S., Komáromi, I., Byun, K. S., Morokuma, K. & Frisch, M. J. A new ONIOM implementation in Gaussian 98. 1. The calculation of Energies, gradients and vibrational frequencies and electric field derivatives. *J. Mol. Struct. (Theochem)*. **462**, 1–21 (1999).
35. Vreven, T. *et al.* Combining quantum mechanics methods with molecular mechanics methods in ONIOM. *J. Chem. Theory and Comput.* **2**, 815–826 (2006).
36. Svensson, M. *et al.* ONIOM: A multilayered integrated MO+MM method for geometry optimizations and single point energy predictions. A test for Diels-Alder reactions and Pt(P(t-Bu)<sub>3</sub>)<sub>2</sub>+H<sub>2</sub> oxidative addition. *J. Phys. Chem.* **100**, 19357–19363 (1996).
37. Svensson, M., Humbel, S. & Morokuma, K. Energetics using the single point IMOMO (integrated molecular orbital plus molecular orbital) calculations: Choices of computational levels and model system. *J. Chem. Phys.* **105**, 3654–3661 (1996).
38. Kozuch, S. & Shaik, S. How to conceptualize catalytic cycles? The energetic span model. *Acc. Chem. Res.* **44**, 101–110 (2010).
39. Briones, J. F. & Huw, H. L. D. Silver triflate-catalyzed cyclopropenation of internal alkynes with donor-/acceptor-substituted diazo compounds. *Org. Lett.* **13**, 3984–3987 (2010).
40. Fisher, L. A. & Fox, J. M. Studies on the stability of cycloprop-2-ene carboxylate dianions and reactions with electrophiles. *J. Org. Chem.* **73**, 8474–8478 (2008).
41. Becke, A. D. Density-functional thermochemistry. III. The role of exact exchange. *J. Chem. Phys.* **98**, 5648–5652 (1993).
42. Lee, C., Yang, W. & Parr, R. G. Development of the Colle-Salvetti correlation-energy formula into a functional of the electron density. *Phys. Rev. B* **37**, 785–789 (1988).
43. Becke, A. D. A new mixing of Hartree-Fock and local density-functional theories. *J. Chem. Phys.* **98**, 1372–1377 (1993).
44. Andrae, D., Häußermann, U., Dolg, M., Stoll, H. & Preuß, H. Energy-adjusted *ab initio* pseudopotentials for the second and third row transition-elements. *Theor. Chim. Acta* **77**, 123–141 (1990).
45. Ribeiro, R. F., Marenich, A. V., Cramer, C. J. & Truhlar, D. G. Use of solution-phase vibrational frequencies in continuum models for the free energy of solvation. *J. Phys. Chem. B* **115**, 14556–14562 (2011).
46. Zhao, Y. & Truhlar, D. G. A new local density functional for main-group thermochemistry, transition metal bonding, thermochemical kinetics, and noncovalent interactions. *J. Chem. Phys.* **125**, 194101 (2006).
47. Marenich, A. V., Cramer, C. J. & Truhlar, D. G. Universal solvation model based on solute electron density and on a continuum model of the solvent defined by the bulk dielectric constant and atomic surface tensions. *J. Phys. Chem. B* **113**, 6378–6396 (2009).
48. Grimme, S., Antony, J., Ehrlich, S. & Krieg, H. A consistent and accurate *ab initio* parametrization of density functional dispersion correction (DFT-D) for the 94 elements H-Pu. *J. Chem. Phys.* **132**, 154104 (2010).
49. Grimme, S. Accurate description of van der Waals complexes by density functional theory including empirical corrections. *J. Comput. Chem.* **25**, 1463–1473 (2004).
50. Zhao, Y. & Truhlar, D. G. The M06 suite of density functionals for main group thermochemistry, thermochemical kinetics, noncovalent interactions, excited states, and transition elements: two new functionals and systematic testing of four M06-class functionals and 12 other functionals. *Theor. Chem. Acc.* **120**, 215–241 (2008).

## Acknowledgements

We are grateful to the Natural Science Foundation of China (Project 21421001), Tianjin Natural Science Foundation (14JCYBJC20100), and MOE Innovation Teams (IRT-13R30 and IRT13022) of China for the financial support of this research. Calculations were performed on the TH-1A cluster at the National Supercomputer Centre in Tianjin, which is supported by the NSFC. We are indebted to Professor Zunsheng Cai for his helpful discussions.

## Author Contributions

C.C.Z. and X.N.K. performed the computations and data analysis. C.C.Z., X.N.K and X.F.X. contributed to the discussions and writing the manuscript.

## Additional Information

**Supplementary information** accompanies this paper at <http://www.nature.com/srep>

**Competing financial interests:** The authors declare no competing financial interests.

**How to cite this article:** Zhou, C.-C. *et al.* Computational Prediction of One-Step Synthesis of Seven-membered Fused Rings by (5+2) Cycloaddition Utilising Cycloalkenes. *Sci. Rep.* **5**, 12272; doi: 10.1038/srep12272 (2015).



This work is licensed under a Creative Commons Attribution 4.0 International License. The images or other third party material in this article are included in the article's Creative Commons license, unless indicated otherwise in the credit line; if the material is not included under the Creative Commons license, users will need to obtain permission from the license holder to reproduce the material. To view a copy of this license, visit <http://creativecommons.org/licenses/by/4.0/>